Submitted to the International Europhysics Conference on High-Energy Physics HEP99,
Tampere, Finland, July 1999.

Measurement of the Production of $D^{*\pm}$ Mesons in Deep-Inelastic Diffractive Interactions at HERA

H1 Collaboration

Abstract

A measurement is presented of $D^{*\pm}$ meson production in diffractive interactions at HERA. The cross section is measured in the kinematic range $2 < Q^2 < 100\ \mathrm{GeV}^2$, $0.05 < y < 0.7$, $x_{I\!P} < 0.04$, $M_Y < 1.6\ \mathrm{GeV}$, $|t| < 1\ \mathrm{GeV}^2$, $p_T(D^{*\pm}) > 2\ \mathrm{GeV}$ and $|\eta(D^{*\pm})| < 1.5$, where M_Y is the mass of the diffractively scattered proton-remnant system and η and p_T are measured in the H1 laboratory frame. The cross section is presented differentially as a function of various kinematic variables, including a hadron level estimate of the fraction of the pomeron's momentum carried by the parton entering the hard-subprocess $z_{I\!P}^{obs}$. The results are compared with a model based on a partonic pomeron as determined in a QCD analysis of the diffractive structure function, with perturbative QCD calculations of two gluon exchange and with a soft colour interaction model.

Abstract: 157ag
Parallel sessions: 3
Plenary sessions: 3

1 Introduction

Large rapidity gap events observed at HERA constitute approximately 10% of the inclusive deep inelastic scattering (DIS) cross section [1]. They are attributed dominantly to pomeron exchange. The rate of diffractive open charm production in DIS is sensitive to the gluon content of the exchange, since charm quarks are predominantly produced by the photon-gluon fusion process (PGF). This paper presents a measurement of differential distributions which explore the dynamics of diffractive charm production. Different theoretical approaches to diffractive charm production exist and are discussed below.

The resolved pomeron model [2] is a partonic interpretation of a factorisable pomeron. The calculation of the cross section factorises into the parton density of the pomeron and a pomeron flux factor, describing the probability for finding a pomeron in the proton. The pomeron flux is motivated by Regge theory and is approximately proportional to $(1/x_{\mathbb{P}})^{1+2\varepsilon}$, where $x_{\mathbb{P}}$ is the fraction of the proton's momentum carried by the pomeron and ε is small. Within this picture, the partonic content of the pomeron has been determined by a QCD analysis of the inclusive diffractive structure function $F_2^{D(3)}(\beta, Q^2, x_{\mathbb{P}})$ [1], where β is the fraction of the momentum of the pomeron carried by the quark interacting with the photon. The parton distributions, obtained from the fit to the data, contain a dominant gluon distribution. Open charm is produced in the resolved pomeron model by PGF (see figure 1a), where the photon, radiated by the incoming lepton, interacts with a gluon of the pomeron, carrying a fraction $z_{\mathbb{P}}$ of the pomeron momentum.

In perturbative QCD diffractive open charm production can be realised by the exchange of two perturbative gluons [3, 4, 5] (see figure 1b). Consequently the cross section for the process $\gamma^* + p \to c\bar{c} + p'$ is approximately proportional to the gluon density squared $[x_{\mathbb{P}} G_p(x_{\mathbb{P}}, \mu)]^2$ of the proton, where μ is the factorisation scale. This process is implemented in the Monte Carlo generator RAPGAP 2.06 [6] allowing for different parameterisations of the gluon density in the proton. Only $c\bar{c}$ final states are included in the model and for a full description $c\bar{c}g$ and higher order Fock states are required.

In the soft colour interaction model (SCI) [7] the $c\bar{c}$ pair is produced via PGF from the gluon distribution of the proton. With a certain probability the colour structure of the partonic final state is changed during the fragmentation phase, as soft gluon exchanges take place between the outgoing charm quarks and the proton remnant. Large rapidity gap events can be produced when the soft interactions lead to net colour-singlet exchange. The probability for SCI is a free parameter in this model, which has been implemented in the Monte Carlo generator AROMA 2.2 [8].

2 Event Selection

The data were collected using the H1 detector [9] over the three years 1995, 1996 and 1997, where HERA collided 27.6 GeV positrons with 820 GeV protons. After rejecting data when parts of the detector essential for the analysis were not operational, the integrated luminosity used is 20.8 pb^{-1}.

The analysis is restricted to events in which the scattered positron is detected and measured in the SPACAL [10], a lead – scintillating fibre spaghetti calorimeter situated in the backward

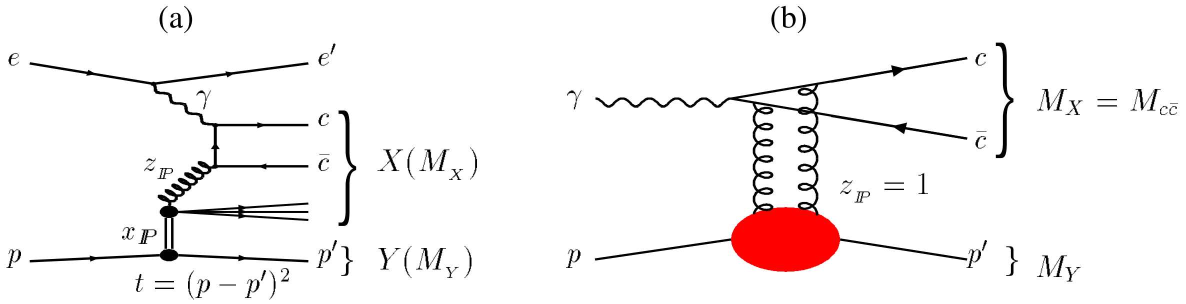

Figure 1: *(a) Photon–gluon fusion in the resolved pomeron process. $z_{I\!P}$ denotes the fraction of the pomeron momentum carried by the gluon. (b) Diffractive open charm production by perturbative two gluon exchange. In this process the mass of system X is restricted to the invariant mass of the $c\bar{c}$ system and thus $z_{I\!P} = 1$ at the parton level always holds.*

region of the H1 detector[1]. The events were triggered by an electromagnetic cluster in the SPACAL, in coincidence with a charged track signal from both the multi-wire proportional chamber (MWPC) and the central drift chamber of the detector. The positrons are identified as clusters with energy $E_e > 9$ GeV, radius < 3.5 cm (consistent with electromagnetic energy deposition), and with the cluster matching within 2.5 cm to a charged track segment in the backward drift chamber BDC [11], located immediately in front of the SPACAL. The polar angle of the scattered electron was required to be $\theta < 177^o$. These requirements restrict the accessible range in Q^2, the negative four-momentum squared of the exchanged photon, and the inelasticity y, defined as $y = p \cdot q / p \cdot k$, where p, k and q are the four-momenta of the incident proton, of the incident positron and of the exchanged photon, respectively. The kinematic region measured is $2 < Q^2 < 100$ GeV^2 and $0.05 < y < 0.7$, where Q^2 and y are calculated from the scattered electron energy and angle.

As with measurements of the diffractive structure function $F_2^{D(3)}$ [1], the hadronic final state is separated into two distinct systems X and Y, respectively of mass M_X and M_Y, lying on either side of the largest gap in rapidity between hadrons in the photon–proton centre of mass frame; the system Y being closest to the outgoing proton direction. Diffractive events are defined experimentally by the absence of any signal in detectors situated in the forward part of the H1 apparatus, which have acceptance at large pseudorapidities[2]. This requirement restricts the mass of the dissociating system $M_Y < 1.6$ GeV and the momentum transfer to the proton $|t| < 1$ GeV^2. The extent of the rapidity gap is measured using the quantity η_{max}, which is the pseudorapidity of the most forward cluster in the liquid argon calorimeter with energy $E > 300$ MeV. A cut of $\eta_{max} < 3.3$ is applied, which restricts the $x_{I\!P}$ range to be less than 0.04.

3 Reconstruction of $D^{*\pm}$ Mesons

The D^{*+} mesons are reconstructed using the decay channel

$$D^{*+} \to D^0 \, \pi^+_{slow} \to (K^- \, \pi^+) \, \pi^+_{slow}, \tag{1}$$

[1]In the following, the z axis is taken along the beam direction, the $+z$ or "forward" direction being that of the outgoing proton beam.

[2]The pseudorapidity, η, of an object detected with polar angle θ is defined as $\eta = -\ln\,\tan(\theta/2)$.

which has a branching ratio of 2.63% [12] (the charge conjugate is always implied).

The decay products are detected in the central tracker. To ensure good detection efficiency and to reduce the combinatorial background, the tracks are required to lie in the angular range $20^o < \theta < 160^o$ and to have a transverse momentum p_T, defined with respect to the beam axis, of at least 140 MeV for the π_{slow} and 250 MeV for both the K and π. To protect further against badly reconstructed tracks, each track is required to be at least 10 cm long in the projection perpendicular to the beam and to start in the inner section of the tracker.

The invariant mass of the $K\pi$ combination has to be consistent with the D^0 mass within ± 80 MeV. After cuts on the direction ($|\eta(D^{*\pm})| < 1.5$) and transverse momentum ($p_T(D^{*\pm}) > 2\ \mathrm{GeV}$) of the $D^{*\pm}$, the mass difference distribution $\Delta M = M(K^-\pi^+\pi^+_{slow}) - M(K^-\pi^+)$ is plotted in figure 2.

The number of $D^{*\pm}$ candidates is determined by fitting the histogram in figure 2 with a Gaussian distribution for the signal plus a background function $a(\Delta M - M_\pi)^b$, where M_π is the mass of the pion. The position of the Gaussian is fixed to a value taken from a higher statistics sample of events where no diffractive cuts were applied [13]. The width and normalisation of the Gaussian and the background parameters a and b are allowed to vary. The number of $D^{*\pm}$ candidates detected is found to be $38 \pm 10\ (\mathrm{stat.}) \pm 4\ (\mathrm{syst.})$, where the systematic error is estimated by varying the details of the fit procedure.

4 Cross Section Calculation

Monte Carlo simulations are used to correct the data for the effects of losses and migrations due to the finite resolution of the reconstruction. The acceptance is calculated by running the H1 detector simulation program on a sample of $D^{*\pm}$ events from the diffractive Monte Carlo generator RAPGAP [6] in the resolved pomeron mode. The RAPGAP program is used to model events in the kinematic range $x_{I\!P} < 0.1$, which contain an elastic proton ($M_{_Y} = m_p$). A background of the order 5% to the selected sample of events arises from interactions with high $x_{I\!P}$ ($x_{I\!P} > 0.1$) or large M_Y ($M_Y > 5$ GeV) values. The contribution of this background is estimated using the heavy quark generator AROMA [8]. The DIFFVM [14] generator, which contains both elastic and proton dissociation events, is used to obtain the correction (of order 4%) for the net smearing of diffractive events about the kinematic boundary of the measurement $M_Y < 1.6\ \mathrm{GeV}$. Another significant source of background is due to contributions to the signal of events with D^0 decay modes other than that defined in (1), with wrongly identified charged particles or lost neutral particles. Simulations using the AROMA Monte Carlo show that this background contributes $3.5 \pm 1.5\%$ of the signal [13]. The contribution from photoproduction background is found to be negligible.

The trigger efficiency for diffractive events of around 85% is obtained from the detector simulation, and is verified in the data using a larger sample of $D^{*\pm}$ candidates without the diffractive conditions. The loss of diffractive events (of order 8%) due to noise fluctuations in the forward detectors is estimated directly from the data, using a sample of random read-outs of the detector, not correlated with a physics trigger.

5 Systematic Errors

Systematic uncertainties in the cross section determination have been estimated by varying the measurement conditions, in particular using the Monte Carlo simulations.

- The largest systematic error is due to uncertainties in the physics model for D^* production used to compute the acceptance corrections. This error is estimated from the difference in the acceptance calculated using the resolved pomeron model and the SCI model which have different underlying kinematic distributions. The error is 18% when averaged over all bins.
- An error of 10% is found for the uncertainty in the fitting procedure used to obtain the number of $D^{*\pm}$ mesons.
- The uncertainty in the reconstruction efficiency of the central tracker for the three tracks is estimated as 7.5%.
- The uncertainty in the trigger efficiency gives a contribution of 6% to the systematic error.
- The uncertainty in the measured energy and angle of the scattered electron leads to a systematic error of 5% when averaged for all bins.
- The uncertainty in the correction due to the smearing of events across the boundary $M_Y = 1.6$ GeV is estimated by varying in the DIFFVM simulation the efficiency of the forward detectors, the assumed M_Y distribution, the ratio of double to single dissociation between 0.5 and 2, and the assumed t dependence. This contributes 6% to the error.
- The uncertainty in the fraction of events lost due to noise in the forward detectors is 6%.
- Other sources of systematic error are the uncertainties in the hadronic energy scale of the liquid argon and SPACAL calorimeters, the uncertainty in the branching ratio for the measured decay channel, and the uncertainties in the $x_{\mathbb{P}}$ and t distributions used in the Monte Carlo simulations to compute acceptances and losses. Each of them is responsible for an error of no more than 5%.

The combined total systematic error on the cross section measurement is 23%.

6 Results

The cross section for the kinematic region $2 < Q^2 < 100\ \mathrm{GeV}^2$, $0.05 < y < 0.7$, $x_{\mathbb{P}} < 0.04$, $M_Y < 1.6\ \mathrm{GeV}$, $|t| < 1\ \mathrm{GeV}^2$, $p_T(D^{*\pm}) > 2\ \mathrm{GeV}$ and $|\eta(D^{*\pm})| < 1.5$ is

$$\sigma(ep \to (D^{*\pm}X)Y) = 154 \pm 40\ (\mathrm{stat.}) \pm 35\ (\mathrm{syst.})\ \mathrm{pb}\ . \tag{2}$$

The cross section is shown differentially as a function of various kinematic variables in figures 3 and 4. The differential cross sections are measured by using a slightly different fitting procedure from that used for the total diffractive cross section described above in section 3. Both the width and the position of the signal Gaussian are fixed to the value obtained from the higher statistics sample of events where no diffractive cuts were applied [13]. This procedure is adopted due to the limited statistics of the differential distributions which typically contain 20 events in each bin. Applying the same procedure to the full diffractive $D^{*\pm}$ sample gives a result consistent with the quoted measurement.

In figure 3 the cross section is shown as a function of p_T^*, $x_{I\!P}$, β (when neglecting t, $\beta \simeq Q^2/(Q^2 + M_X^2)$), and the hadronic observable $z_{I\!P}^{obs}$. Here, p_T^* is the transverse momentum of the $D^{*\pm}$ in the $\gamma^* p$ centre of mass system. The observable $z_{I\!P}^{obs}$ is an approximation (in the resolved pomeron picture) to the momentum fraction of the pomeron carried by the interacting gluon $z_{I\!P}$ which is defined by the equation

$$z_{I\!P} = \beta \cdot \left(1 + \frac{M_{c\bar{c}}^2}{Q^2}\right) \simeq \frac{M_{c\bar{c}}^2 + Q^2}{M_X^2 + Q^2},$$

where $M_{c\bar{c}}$ is the centre of mass energy of the $c\bar{c}$ system. $M_{c\bar{c}}$ can be reconstructed using the scattered positron and the tagged $D^{*\pm}$ meson (see also [13]). If the partons could be observed directly, in the two gluon model $z_{I\!P} = 1$ would always hold. Hadronisation typically leads to a small reduction in $z_{I\!P}$, so that $z_{I\!P} < 1$ at the hadron level. In figure 4 cross sections are also shown as a function of η, Q^2 and y.

The resolved pomeron approach reproduces well the shape of the spectra and in particular the fact that the data show a sizable fraction of charm production in the low $z_{I\!P}^{obs}$ region. However, the model fails in the overall normalisation by a factor of 2 to 3, depending on the choice of hadronisation and factorisation scales and the mass of the charm quark used for the calculation.

The two gluon model for exclusive charm production $\gamma^* + p \to c\bar{c} + p'$, in contrast to the resolved pomeron model, does not describe the regions of higher mass for the system X i.e. low $M_{c\bar{c}}/M_X$, low $z_{I\!P}^{obs}$. It is apparent, also from the p_T^* distribution, that higher order contributions such as $\gamma^* + p \to c\bar{c}g + p'$ are needed. The discrepancy at low β reflects the behaviour at high $x_{I\!P}$. It is, however, interesting to note that the data in regions where the hadronic system X predominantly consists of the $c\bar{c}$ system alone (e.g. high $z_{I\!P}^{obs}$) are well reproduced in magnitude.

The SCI model fails in the overall normalisation by a factor of about 2 but reproduces reasonably well the shape of the differential distributions.

7 Conclusion

The dynamics of diffractive charm production have been studied. The measured cross section is below the expectation based on the resolved pomeron model with parton distributions derived from the QCD analysis of inclusive diffractive DIS data. Differential cross sections have been presented, which are able to discriminate between different models. They are all well described in shape by the resolved pomeron model and reasonably well by the SCI model.

References

[1] C. Adloff et al., H1 Coll., Z.Phys. **C76** (1997) 613.

[2] G. Ingelmann, P.E. Schlein *Phys. Lett.* B **152**, 1985 (256)

[3] J. Bartels, H. Lotter, M. Wüsthoff, *Phys. Lett.* B **379**, 1996 (239)

[4] J. Bartels, C. Ewerz, H. Lotter, M. Wüsthoff, *Phys. Lett.* B **386**, 1996 (389)

[5] H. Lotter, *Phys. Lett.* B **406**, 1997 (171)

[6] H. Jung, *Comput. Phys. Commun.* **86**, 1995 (147);
(for update see http://www-h1.desy.de/ jung/rapgap/rapgap.html)

[7] A. Edin, G. Ingelman, J. Rathsman, *Z. Phys.* C **75**, 1997 (57), *Phys. Rev.* D **56**, 1997 (7317)

[8] G. Ingelman, J. Rathsman, G.A. Schuler *Comput. Phys. Commun.* **101**, 1997 (135)

[9] I. Abt et al., H1 Coll., Nucl. Instr. and Meth. **A386** (1997) 310-347 and 348-396.

[10] R.D. Appuhn *et al* (H1 SpaCal group), DESY preprint 96-171

[11] H1 collaboration, Technical proposal for the upgrade of the backward region of the H1 detector, DESY internal report PRC-93/02.

[12] C. Caso *et al.* (Particle Data Group), Eur. Phys J. **C3** (1998) 1.

[13] H1-Collaboration., S. Adloff et al., *Nucl. Phys.* B **545**, 1999 (21)

[14] B. List, *Diffraktive J/ψ-Produktion in Elektron-Proton-Stöβen am Speicherring HERA*, Diploma Thesis, Techn. Univ. Berlin, 1993 (unpubl.).

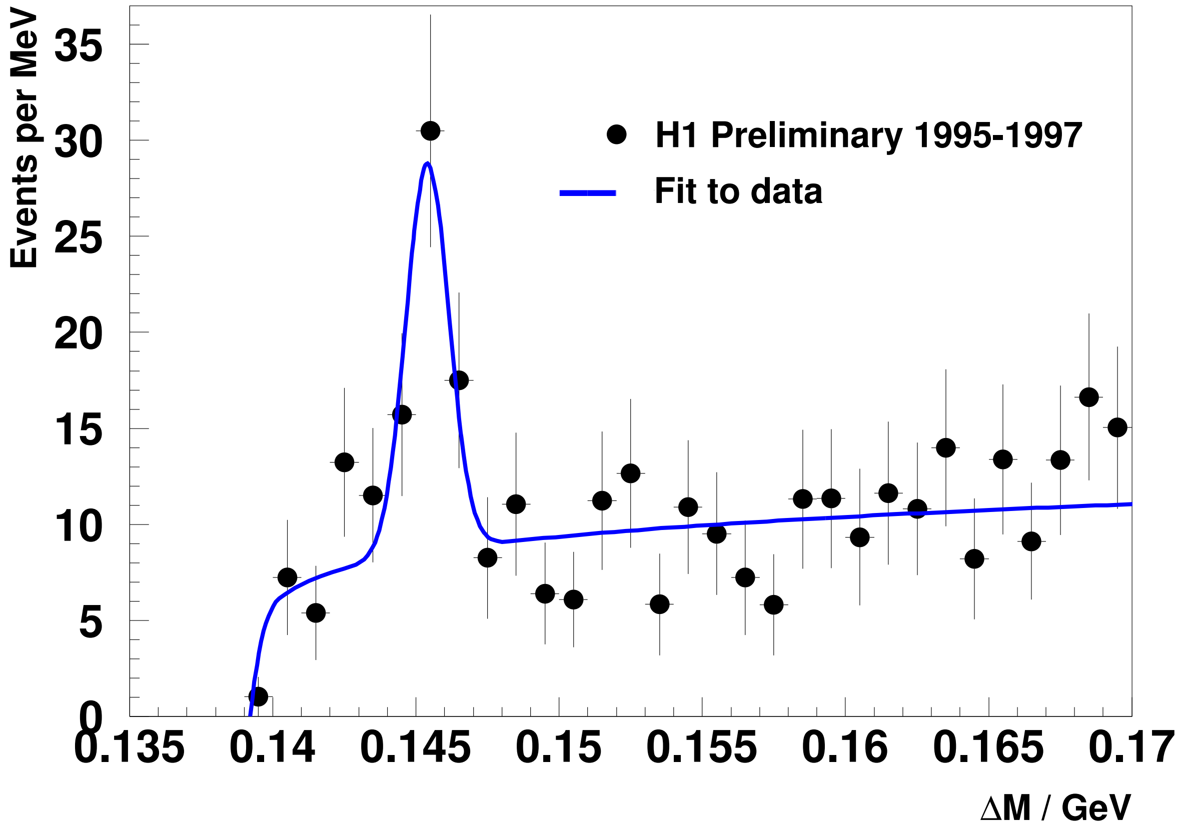

Figure 2: *Distribution of the mass difference* $\Delta M = M(K^-\pi^+\pi^+_{slow}) - M(K^-\pi^+)$*, with a curve fitted to the form* $a(\Delta M - M_{\pi^+})^b + Gaussian$*. The number of* $D^{*\pm}$ *mesons in the Gaussian part of the fit is* $38 \pm 10\ (\mathrm{stat.}) \pm 4\ (\mathrm{syst.})$.

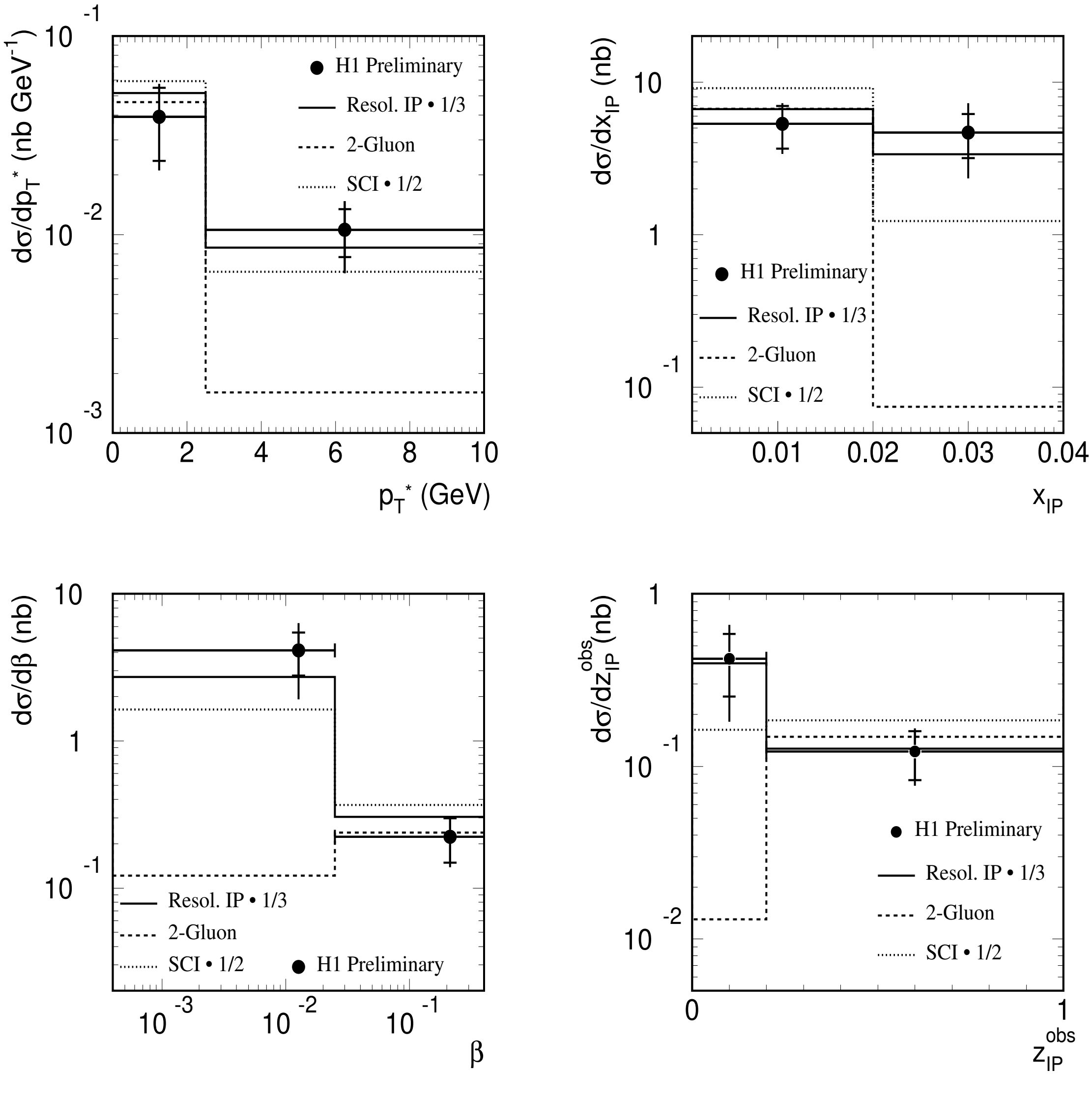

Figure 3: *Cross sections $\sigma(ep \to e(D^{*\pm}X)Y)$ as a function of p_T^*, where p_T^* denotes the transverse momentum of the $D^{*\pm}$ in the $\gamma^* p$ centre of mass system, the fraction $x_{\mathbb{P}}$ of the proton momentum carried by the pomeron, β which is equal to $x/x_{\mathbb{P}}$ and $z_{\mathbb{P}}^{obs}$, which is an approximation to the momentum fraction of the pomeron carried by the gluon entering the hard interaction. The cross sections are measured in the kinematic range $2 < Q^2 < 100\ \mathrm{GeV}^2$, $0.05 < y < 0.7$, $x_{\mathbb{P}} < 0.04$, $M_Y < 1.6\ \mathrm{GeV}$, $|t| < 1\ \mathrm{GeV}^2$, $p_T(D^{*\pm}) > 2\ \mathrm{GeV}$ and $|\eta(D^{*\pm})| < 1.5$. The data are points with error bars (inner: statistical, outer: total) and are compared to the resolved pomeron model (solid line), the 2–gluon model (dashed line) and the SCI–model (dotted line). The resolved pomeron model is normalised by a factor of $1/3$ and the SCI–model by a factor of $1/2$.*

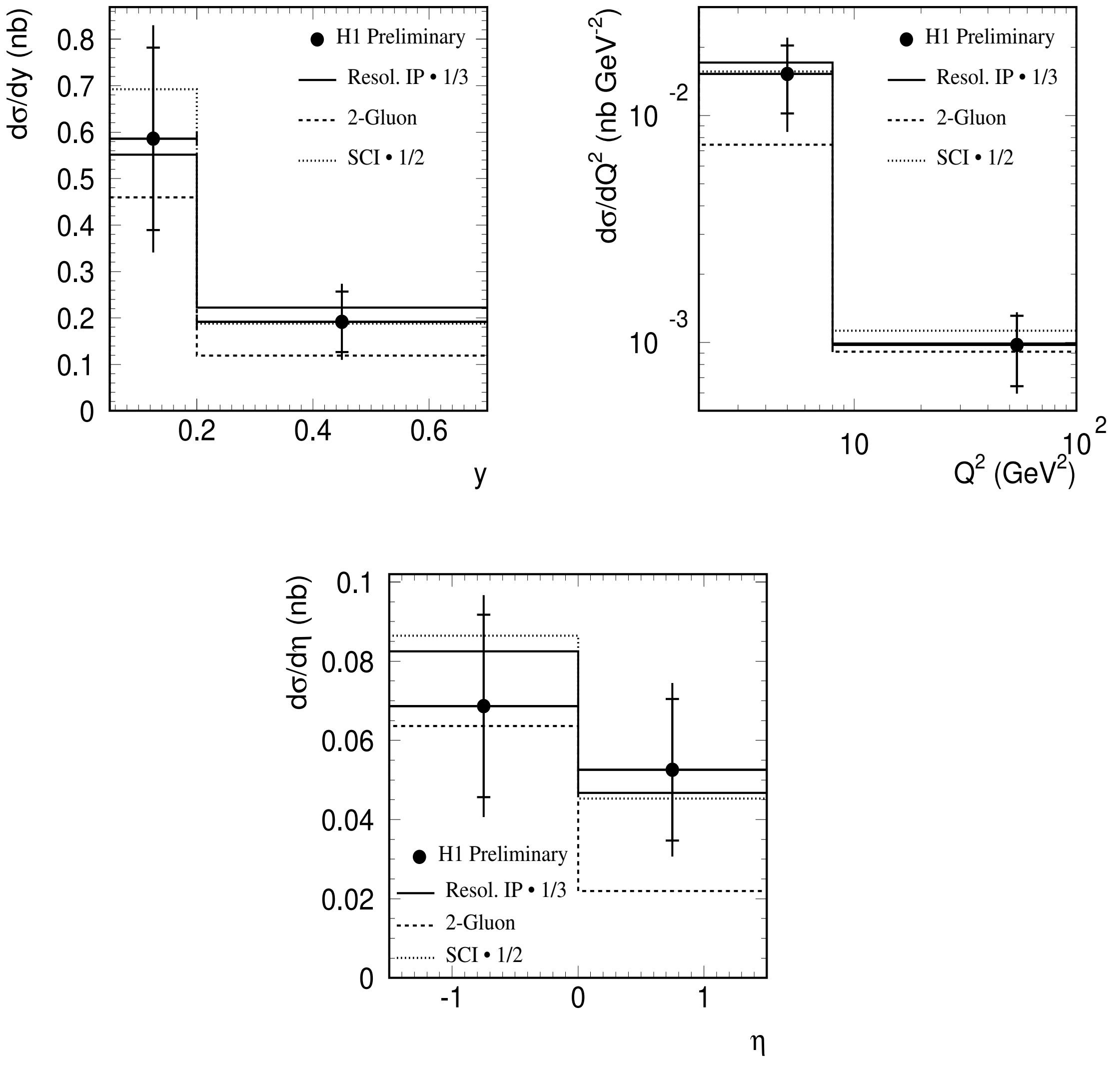

Figure 4: *Cross sections* $\sigma(ep \to e(D^{*\pm}X)Y)$ *as a function of* y*,* Q^2 *and* η*. The cross sections are measured in the kinematic range* $2 < Q^2 < 100\ \mathrm{GeV}^2$*,* $0.05 < y < 0.7$*,* $x_{I\!P} < 0.04$*,* $M_Y < 1.6\ \mathrm{GeV}$*,* $|t| < 1\ \mathrm{GeV}^2$*,* $p_T(D^{*\pm}) > 2\ \mathrm{GeV}$ *and* $|\eta(D^{*\pm})| < 1.5$*. The data are points with error bars (inner: statistical, outer: total) and are compared to the resolved pomeron model (solid line), the 2–gluon model (dashed line) and the SCI–model (dotted line). The resolved pomeron model is normalised by a factor of* $1/3$ *and the SCI–model by a factor of* $1/2$*.*